The Egyptian Journal of Remote Sensing and Space Sciences 25 (2022) 609–620

HOSTED BY

ELSEVIER

Contents lists available at ScienceDirect

The Egyptian Journal of Remote Sensing and Space Sciences

journal homepage: www.sciencedirect.com

Impact of anthropogenic activities on urban heat islands in major cities of El-Minya Governorate, Egypt

Kamel Mansour [a,*], Mohamed Alkhuzamy Aziz [b], Seham Hashim [c], Hala Effat [a]

[a] Environmental Studies and Land Use Division, National Authority for Remote Sensing and Space Sciences (NARSS), Egypt
[b] Faculty of Social and Human Sciences, Galala University and Faculty of Arts Fayoum University, Egypt
[c] Department of Geography, Faculty of Women for Arts, Science and Education, Ain Shams University, Egypt

ARTICLE INFO

Article history:
Received 2 October 2021
Revised 7 March 2022
Accepted 29 March 2022
Available online 7 April 2022

Keywords:
Urban heat island
Land surface temperature
Spectral INDICES
El-Minya cities
Landsat imagery

ABSTRACT

Urban heat islands (UHIs) represent one of the significant factors in regard to environmental and human health. UHIs are significantly changeable, responding to the land use type and the dominant anthropogenic activities. In this research, UHIs in El-Minya cities were identified based on Land Surface Temperature (LST) measurements. Thermal bands of Landsat imagery were processed to produce LST in the cities of El-Minya governorate in 2001, 2011, and 2021. In addition, the spectral indices; Normalized Difference Vegetation Index (NDVI), the Modified Normalized Difference Water Index (MNDWI), and the Normalized Difference Built-up Index (NDBI) were retrieved from the processing of multispectral Landsat imagery to assess different Land-cover units in the study area and to detect their correlation with LST/UHIs. Analysis of data indicated that LST variations are corresponding with different land-cover types. It was found that NDVI and NDWI have a strong negative influence on LST (R = −0.7 and −0.8 for both indices, respectively), while NDBI has a significant positive correlation (R = 0.85). Furthermore, the highest LST was detected at the cities of El-Minya, New-El-Minya, and Malawi, consequently. These regions have the greatest potential for UHIs formation among other El-Minya governorate cities. The year 2021 recorded the highest average LST with a value of 34.1 °C where the largest UHI area was observed in New-El-Minya (2.74Km^2) in 2001, and (2.6 Km^2) in 2021, as well as (1.12Km^2) in El-Minya in 2011. It can be concluded that increasing LST and UHIs at different districts of El-Minya arise from urbanization and industrialization processes.

1. Introduction

Growing urbanization and industrialization increase environmental issues like air quality deterioration and rising temperature (Sigman, et al., 2012; El-Zeiny et al., 2022). Urban heat island (UHI) represents the higher temperature in urban regions compared with its non-urban surroundings. It is considered a main feature of urban climatology (Huang and Lu, 2018), which leads to great anthropogenic variations in the Earth's environments (Oke, 1982). The UHIs formation is enhanced in urban regions as a result of replacing the evaporative vegetation surfaces with impermeable surfaces, besides releasing anthropogenic heat (Rizwan et al., 2008).

Detection of the Surface UHIs is mainly relying on the Land Surface Temperature (LST), which has a direct effect on the air temperature through energy exchange between the earth and atmosphere (Zhou, et al., 2019). Multi-temporal thermal remote sensing can measure the surface's temperature (LST) and enables the study of urban thermal environments at varied spatial and temporal resolutions (Voogt and Oke, 2003; Deilami et al., 2018).

UHIs affect the environment through the alternation of regional climate (Shepherd, 2005), flora (Zhao et al., 2016), water/air quality (Grimm et al., 2008), and energy usage (Santamouris et al., 2015). However, human exposure to extreme heat creates thermal stress and leads to sunstroke, dehydration, hyperthermia, heat-stroke and may increase morbidity and mortality rates (Patz et al., 2005). Nearly 55% of the world's inhabitants reside in urbanized regions (UN, 2018); they might be exposed to these UHIs consequent risks, particularly, the elderly, infants, children, and sick individuals (Kovats and Hajat, 2008). Generally, urbanization is

Peer review under responsibility of National Authority for Remote Sensing and Space Sciences.
* Corresponding author at: Environmental Studies and Land Use Division, National Authority for Remote Sensing and Space Sciences (NARSS), Cairo, Egypt.
E-mail addresses: kmansour339@gmail.com, kame.fathi@narss.sci.eg (K. Mansour), Prof.Aziz@gu.edu.eg, maz55@fayoum.edu.eg (M.A. Aziz), seham.hashim@women.asu.edu.eg (S. Hashim), haeffat@yahoo.com (H. Effat).

https://doi.org/10.1016/j.ejrs.2022.03.014
1110-9823/

occurring at a surpassing rate globally, the modification in urban areas leads to changing the atmospheric environment at different geographic scales (Li et al., 2011). The UHI could be more serious under the warming climate conditions in the rapidly developing world (Seto et al., 2012).

Monitoring LST and UHIs using multi-temporal thermal remote sensing imagery have received increasingly greater attention in recent years due to their impacts on the urban environment (e.g., Peng et al., 2012; Clinton and Gong, 2013; Li et al., 2017; Huang and Lu, 2018; Roupioz et al., 2018, Renard et al., 2019; Miky, 2019, Faisal, et al., 2021, Liu et al., 2022). Chen et al. (2006) analyzed Landsat images to estimate brightness temperatures and identify the land-use/cover based on different biophysical indices.

As well, Roupioz et al. (2018) studied the potentiality of using satellite data to examine the UHIs depending on LST and emissivity measurement from various thermal-infrared (TIR) data sources. In addition, the LST of the major redeveloped urban areas in Lyon-France was studied by Renard et al., (2019) and correlated with different land-use and spectral indices using Landsat data (Elbeih and El-Zeiny, 2018).

Several studies were carried out to understand the UHI and its serious impacts on the environment and humans in Egypt. For instance, Effat et al. (2014) explored the dynamics of UHIs development and its correlation with different land-use in Tanta city. As well, AbouEl-Magd et al. (2016) studied the UHIs over Cairo using multi-temporal Landsat data; they proved that urban encroachment over cultivated lands raised UHIs formation. El-Zeiny and Effat (2017) discussed the remote sensing and GIS ability to monitor LST in El-Fayoum governorate.

Recently, cities are fighting to adapt the climatic changes by applying many actions to evolve human life quality and comfort. Thus, this study aims at detecting UHIs in 10-major cities of El-Minya Governorate, Egypt, namely, "El-Minya City, El-Fikrih City, Mallawi City, Dirmouas City, Samalut City, Bani-Mazar City, Magagh City, El-Adwa City, New-El-Minya City, Matai City" using earth observations and GIS techniques. In addition, it investigates the relationship between surface temperature and land-use/cover indicated by different spectral indices including; NDVI, NDBI, and MNDWI.

2. Materials and methods

2.1. Study area

El-Minya Governorate is enclosed by Benisuef Governorate from the north, Assiut and New-Valley Governorates from the south, Red Sea governorate from the east, and Giza Governorate from the west (ELDeeb et al., 2015). Fig. 1 shows the location map of El-Minya Governorate with the administrative boundaries of each city. El-Minya is bounded from the east and west by 2-elevated calcareous plateaus, splitting from the center by the Nile River. The Nile flows along the western region of the valley leading to increasing vegetated land in the west than the east.

El-Minya is one of Upper Egypt's most densely populated governorates, with a total area of 32279Km^2 and a population count reached 6,033,000 censuses (CAPMAS-March-2021: https://www.capmas.gov.eg/). The governorate is divided administratively into 9-districts (Markaz), 57-local units, 346-villages, 1429-small-villages and Naga besides New-El-Minya city (El-Bayomi and Ali, 2015). The districts include, from north to south, El-Adwa, Maghagha, Bani-Mazar, Matai, Samalout, El-Minya (the capital), Abu-Qirqas, Mallawi, and Dirmouas. The study area has an arid to semi-arid climate with prevailing dry warm summer, and mild with scarce rainfall in winter (Abdel-Moneim et al., 2016). Throughout January, the mean temperature is nearly 4.5–20.5 °C, exceeding 40.0 °C within summer. Relative humidity fluctuates from 68% in January to more than 70% in June (Attia, 1974).

2.2. Data used

To quantitatively estimate the LST in El-Minya in this study, Landsat TM and OLI images acquired on 17th July 2001, 28th July 2011, and 8th July 2021 were analyzed. The study area is located in 2-Landsat scenes; consequently, 6-images were downloaded from the US Geological Survey (USGS), Earth Resource Observation Systems Data Center (http://glovis.usgs.gov/). All of the selected images are nearly cloud-free.

2.3. Pre-processing techniques

Image pre-processing is essential for satellite data analysis, particularly thermal-IR data to reduce noise, enhance the image's quality and eliminate geometric, radiometric, and atmospheric errors created during the imaging operation. In this research, atmospheric and geometric correction procedures were applied using the Universal Transverse Mercator (UTM), Datum (WGS84), and Zone (36). In addition, the multispectral bands were mosaicked, followed by masking the 10-cities from the whole image. For the thermal bands, estimation of LST was performed firstly before mosaicking and clipping to avoid any changes in the image DN values.

2.4. Processing techniques

2.4.1. Derivation of at-sensor brightness temperature

Thermal Landsat data (band-6 from Landsat-TM, bands 10 and 11 from Landsat-8) were used to retrieve at-sensor brightness temperature through two steps including, 1) converting digital-number (DN) received by the thermal sensors to spectral radiance [(L_λ-W/(m^2.Sr.µm)] using the following equation (Li et al., 2011).

$$L_\lambda = L_{min} + \frac{(L_{max} - L_{min})}{(Q_{calmax} - Q_{calmin})}(Q_{calDN} - Q_{calmin}) \quad (1)$$

where, $L_{min\lambda}$: minimum radiance, $L_{max\lambda}$: maximum radiance, Q_{calDN}: thermal-band DN value. Q_{calmin}: minimum quantized calibrated pixel value corresponding to $L_{min\lambda}$. Q_{calmax}: maximum quantized calibrated pixel value corresponding to $L_{max\lambda}$.

followed by 2) converting the spectral radiance to at-sensor brightness temperature (T_b). This can be computed by inverting the Plank's function showed in equation-2 (Zhang et al., 2007).

$T_b = \frac{K_2}{Ln(\frac{K_1}{L_\lambda}+1)}$ (2).where the calibration constants K_1 = 1282.71 K and K_2 = 666.09 W.m^{-2}.sr^{-1}.µm^{-1}.

The estimated at-sensor brightness temperature represents the temperature that a blackbody could acquire to generate the same radiance at the same wavelength, it has quite different properties than the real objects (Li et al., 2012). Hence, further correction is required by considering the spectral emissivity of the surface to explicate the non-symmetrical emissivity of different objects (Stathopoulou and Cartalis, 2007). In this research, the emissivity correction procedure is carried out by estimating the NDVI (Sobrino and Raissouni, 2000). In the case of NDVI having values less than 0.2 the pixel is considered a non-vegetated area, while NDVI with values more than 0.5 is considered a fully vegetated area, and has assumed emissivity (0.99). NDVI with values 0.2–0.5 is considered a mix of non-vegetated to highly vegetated zones (Sobrino et al., 2004; Li et al., 2011), thus emissivity is retrieved by equation-3:

$$\varepsilon = \varepsilon_v F_v + \varepsilon_u(1 - F_v) + d\varepsilon. \quad (3)$$

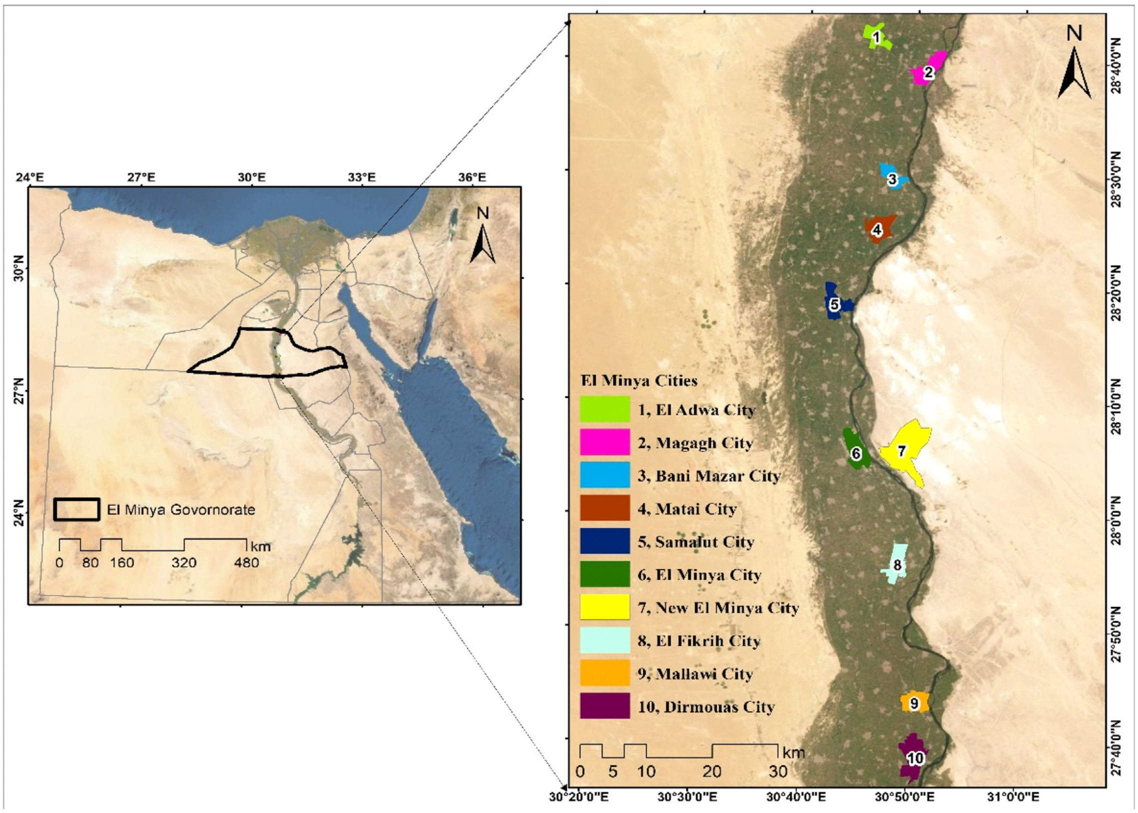

Fig. 1. Location map of El-Minya Governorate with the administrative boundaries of each city.

$$F_v = \left(\frac{NDVI - NDVI_{min}}{NDVI_{max} - NDVI_{min}}\right)2 \quad (4)$$

$$d\varepsilon = (1 - \varepsilon_u)(1 - F_v)F\varepsilon_v. \quad (5)$$

where, ε_v and ε_u are the emissivity of vegetation and built-up surfaces, respectively. F_v is the vegetation ration, $NDVI_{max,}$ and $NDVI_{min}$ indicate the NDVI values in highly vegetated and non-vegetated regions, $d\varepsilon$ substitutes the effect of the geometrical distribution of natural surfaces and the internal reflections, F is a shape factor with a mean value, assuming different geometrical distributions, equals 0.55 (Sobrino et al., 1990; Sobrino et al., 2004).

2.4.2. Retrieval of land surface temperature

The land surface temperature was calculated from formula-6 in kelvin degrees (Artis and Carnahan, 1982; Li et al., 2012; Shahfahad, et al., 2022), and converted to Celsius degrees through formula-7.

$$T_s = \frac{T_b}{1 + (\lambda T_b / \propto) ln\varepsilon} \quad (6)$$

$$T_{(^\circ c)} = T_{(^\circ K)} - 273.15 \quad (7)$$

where, T_s = surface radiant temperature (°K), λ = wavelength, $\propto$= hc/K (1.438×10^{-2} mK), h = Planck constant (6.626×10^{-34} Js^{-1}), C = light velocity (2.998×108 ms^{-1}), K = Boltzman constant ($1.38 \times 10^{-23} JK^{-1}$).

2.4.3. Detection of the UHIs

In order to identify the UHIs, LST data were analyzed statistically to detect the regions with higher LST than their surroundings according to Zhang et al. (2007). Thus, the mean LST value (LST_{mean}) plus one standard deviation (LST_{STD}) was used as a threshold value to define the UHIs for each year in El-Minya cities (equation-8).

$$UHI = LST_{mean} + STD \quad (8)$$

2.4.4. Computation of spectral indices

The widely employed Spectral Indices are reliable indicators for closely observing Earth surfaces using remote sensing technology (Ramaiah, et al., 2020). By using multi-temporal Landsat-8 imagery, spectral indices could be detected and help us to understand the changes in LULC, urban expansion patterns as well as its impacts on land surface temperature (El-Zeiny, 2022). The NDVI was calculated to recognize the vegetated regions by doing a ratio between the reflectance values of near-infrared (NIR) and red (R) bands of Landsat imagery (equation-9) (Lu et al., 2009).

$$NDVI = \frac{NIR - R}{NIR + R} \quad (9)$$

The NDBI was applied to isolate the built-up land from urban areas, based on a ratio between the middle-infrared (MIR) and NIR bands of Landsat data (equation-10) (Liu and Zhang, 2011).

$$NDBI = \frac{MIR - NIR}{MIR + NIR} \quad (10)$$

Furthermore, the MNDWI was used to delineate the open water features by applying a ratio between the MIR and Green (G) bands of Landsat data (equation-11) (Xu, 2006).

$$MNDWI = \frac{G - MIR}{G + MIR} \quad (11)$$

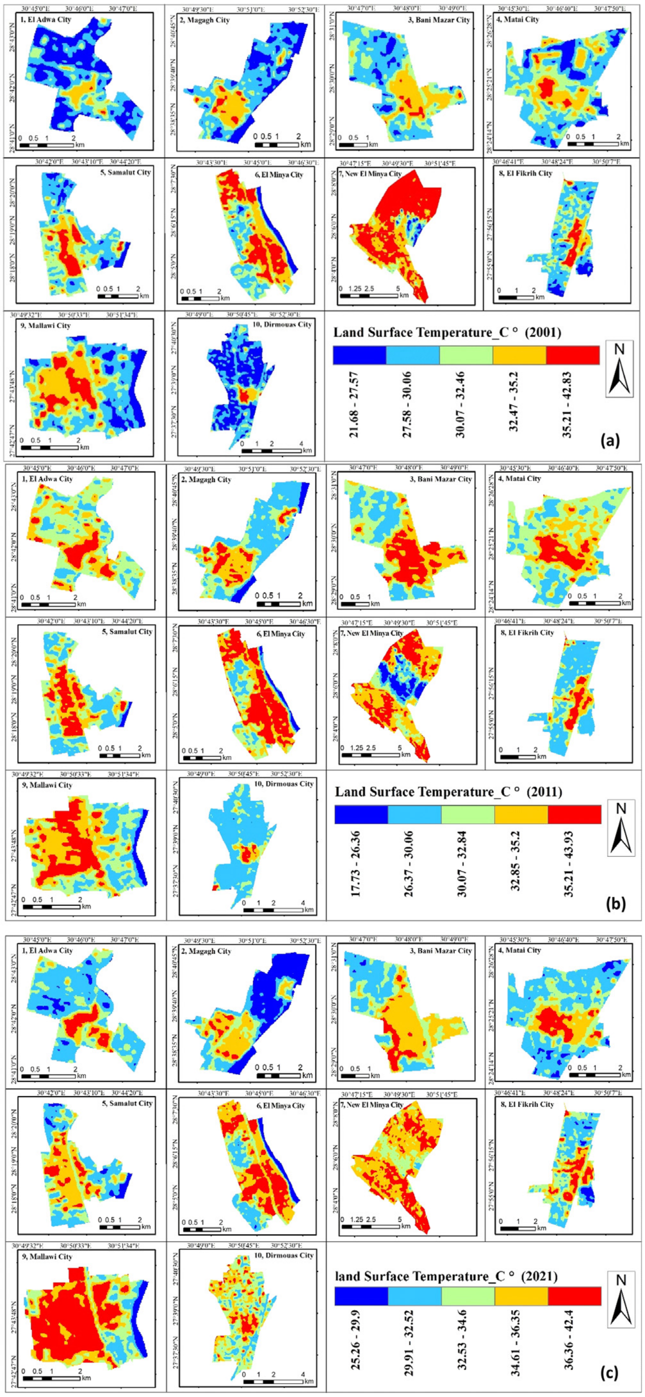

Fig. 2. Spatial distribution maps of LST (°C) in El-Minya cities in a)2001, b)2011, and c)2021.

3. Results and discussion

3.1. Estimation of LST

Analyzing LST during the past 20 years (2001–2021) showed that areas of high LST in 2001 were concentrated in the cities of El-Minya, New-El-Minya, and Mallawi while other cities have low-moderate LST. Fig. 2 shows the LST distribution for the 10-cities of El-Minya Governorate during the period of investigation. In 2011, the regions with high LST are located in El-Minya, New-El-Minya, Mallawi, Samallot, and Bani-Mazar. Recently in 2021, the highest LST was found in the cities of El-Minya, New-El-Minya, and Mallawi. Among the three dates, El-Minya, and New-El-Minya cities registered the highest temperatures nearly 40–44 °C. The year 2021 has the highest mean LST with a value of 34.1 °C, while the lowest LST was recorded in 2001 (31.4 °C). The minimum observed LST was 21.7 °C, 17.7 °C, and 25.3 °C, while the maximum recorded LST was 42.8 °C, 43.9 °C, and 42.4 °C in 2001, 2011, and 2021, respectively. On contrary, the cities of Dirmouas, Matai, and El-Adwa showed slightly lower LST values. Table 1 explores the LST statistics for each city within the period of investigation. The retrieved LST were compared with air temperature measurements at 2-meters height on the same time and location. As shown in Table 2, the maximum air temperature (obtained from MERRA-2) was 39.8 °C, 40.6 °C and 39.9 °C in 2001, 2011, and 2021, respectively.

The observed high LST returns to the effect of built-up areas and road networks as well as wide space for industrial activities, except for New-El-Minya city which is a newly constructed city and has a wide space of desert/bare land. Furthermore, the eastern part of the Nile bank at El-Minya city is a mountainous and valleys region, mainly composed of limestone, marl, and clay rocks (Abdelaal et al., 2017). The construction and composition materials in these urban areas (e.g., bricks and concrete), and bare land/desert have high radiant temperature and low albedo, which lead to absorbing most of the incoming solar radiation and reradiating it back at night as longwave radiation. Their high efficiency in energy storage leads to increase surface temperature.

On the other hand, low LST resulted from the effect of vegetation cover and water (Nile River and Canals) which reduce the

Table 2
Statistics of LST and air temperature (Air T) in degree Celsius (°C) in El-Minya governorate in 2001, 2011, and 2021.

Year	2001		2011		2021	
	LST	Air T	LST	Air T	LST	Air T
MIN.	21.7	24.2	17.7	24.1	25.3	24.4
MAX.	42.8	39.8	43.9	40.6	42.4	39.9
Mean	31.4	32.0	31.9	32.3	34.1	32.1

Table 1
Statistics of LST in degree Celsius (°C) for El-Minya Cities in 2001, 2011, and 2021.

City Stats	2001				2011				2021			
	MIN	MAX	Mean	STD	MIN	MAX	Mean	STD	MIN	MAX	Mean	STD
El-Minya	22.54	42.83	32.59	3.50	24.67	43.57	33.62	3.18	25.75	42.00	34.65	2.75
El-Fikrih	24.67	42.46	30.57	2.81	26.35	42.83	30.72	2.76	28.11	39.92	33.37	2.23
Mallawi	21.68	40.96	30.93	3.42	23.83	41.34	32.71	3.03	25.27	42.40	35.44	2.95
Dirmouas	24.67	37.16	28.15	2.13	26.35	41.71	29.36	2.10	29.83	39.89	34.20	1.61
Samalut	22.54	39.45	30.95	2.94	24.67	41.71	32.04	2.75	25.63	40.49	33.54	2.44
Bani-Mazar	25.10	37.16	30.60	2.35	27.60	39.83	32.55	2.63	29.38	39.41	33.95	1.98
Magagh	22.54	39.45	29.27	3.04	24.25	40.21	30.84	2.92	25.26	39.14	31.56	3.12
El-Adwa	23.40	36.00	28.25	2.44	27.60	37.55	32.22	2.06	29.11	38.84	32.51	2.06
New-El-Minya	21.68	40.21	35.00	2.39	17.73	43.93	32.57	3.89	30.23	41.76	35.77	1.18
Matai	25.10	37.16	30.48	2.51	26.77	37.93	31.99	2.16	28.29	39.50	32.82	2.05

thermal load in the region. Vegetation reduces temperature due to the evapotranspiration and photosynthesis processes that assist in absorbing a large portion of the incident solar radiation and increases the latent heat fluxes, moisture, and surface permeability (Kumar et al., 2012). Gao (1993) revealed that green areas can decrease air temperatures by about 2 °C. In addition, water with its high heat capacity can evaporate from the surface and reduce temperature. These results are consistent with Li et al. (2012) and Miky (2019) who disclosed that urban/built-up/roads areas exhibited the largest LST followed by bare land, while the lowest LST was detected in water surfaces and cultivated land.

3.2. Detection of UHIs

Fig. 3 shows the UHI maps for each city during the analysis period. Results suggested that the spatial distribution of high LST and UHIs is a scattered pattern over built-up areas, semi-bare and barelands as well as limestone deposits along the eastern side of the river at New-El-Minya city. Similar to high LST, UHIs were concentrated in the cities of El-Minya, New-El-Minya, and Mallawi. The maximum UHI area is changeable reporting 2.74 Km^2 in New-El-Minya, 1.12 Km^2 in El-Minya, and 2.6 Km^2 in New-El-Minya again, in 2001, 2011, and 2021, respectively. Table 3 explores the estimated area of UHIs in each city. The cities of Bani-Mazar, Dirmouas, El-Adwa, Magagh, and Matai have a low potentiality for UHI formation and very low area. This returns to the different land cover types that influence energy storage and temperature as well.

Results disclosed that some regions with UHIs in 2001 disappeared in 2021 and vice versa. For example, in Fig. 4(a), in Mallawi city, UHIs appeared in two regions in the north and the south in 2021, while in 2011 there was no presence of UHIs. As explored in the figure these regions were used as agricultural land in the past and then converted to urban areas in 2021. The area has some buildings and a region under development. This plays a role in intensifying the LST and presence of UHIs. Furthermore, the industrial areas enhance the UHIs formation as in El-Fikrih city (Fig. 4b) where the UHI area was observed at the Sugar Factory of Abu-Qirqas, in addition to the other industrial complexes in El-Minya city (such as grinding marble) and Mallawi city (e.g. food, sugar and spinning).

3.3. Correlation between LST and spectral indices

The derived spectral indices provide significant information on LST and UHIs occurrence in the study area considering NDVI (Fig. 5), MNDWI (Fig. 6), and NDBI (Fig. 9) are representing vegetation, water/moisture, and urban/built-up areas, respectively. The overall mean values of these indices are 0.59, 0.4, and −0.12 for NDVI, MNDWI, and NDBI, respectively. Table 4 explores the statistics of NDVI.

Relationships among LST, UHIs, and the spectral indices revealed that regions with elevated LST values have low NDVI and MNDWI. The land-cover type influences not only the LST but also the UHI formation. Consequently, the UHIs are rarely abundant over these land-cover types due to their influence on cooling the surface. A significant negative correlation was observed between LST and NDVI with a correlation coefficient (R = -0.7) and coefficient of determination (R^2 = 0.8). As well, MNDWI is negatively correlated with LST (R = -0.8) (Fig. 7& Fig. 8) which is matching with Kumar et al. (2012). Further, several built-up and some bare-land regions had positive values same as water and moisture which returns to the noise caused by built-up land and desert in the infrared region as explored in Xu (2006).

In contrast, NDBI has a strong positive correlation with the LST and UHIs with a correlation coefficient (R = 0.85) and coefficient of determination (R^2 = 0.7) as shown in Figs. 9 and 10. The areas char-

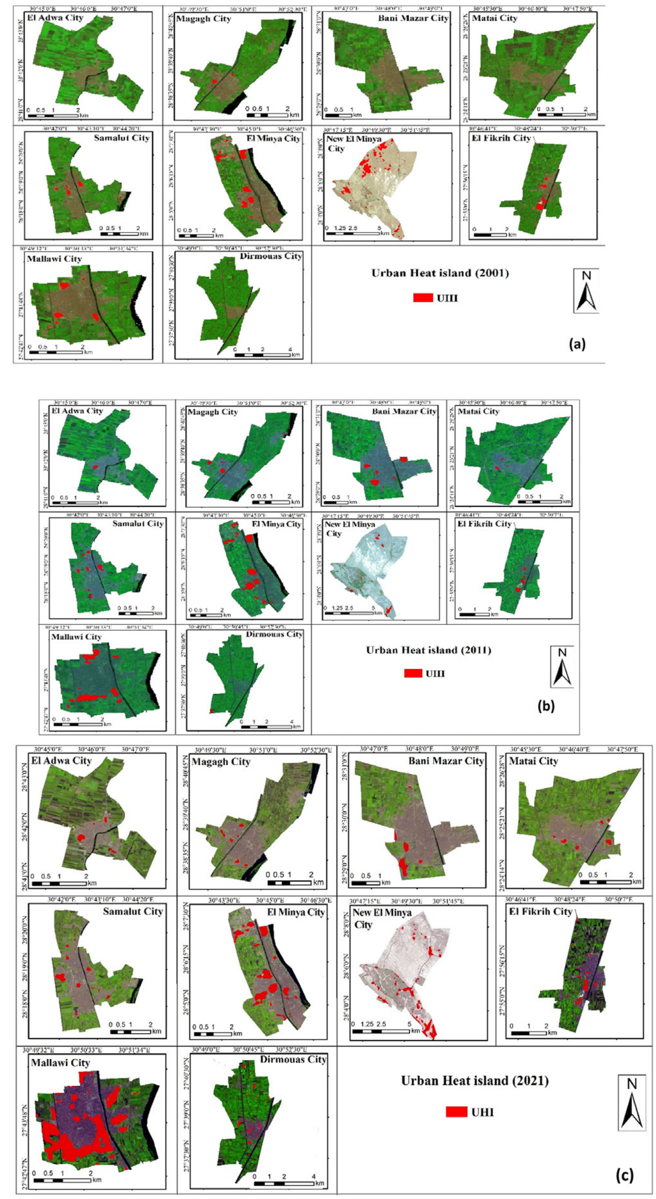

Fig. 3. UHIs in El-Minya cities extracted from LST data in a)2001, b)2011 and c) 2021. The used base maps in the three figures are the Landsat-TM and Landsat-8 captured at the same time of LST/UHIs retrieval.

Table 3
The estimated area (Km^2) of UHI in El-Minya cities in 2001, 2011, and 2021.

City Area	UHI area/Km^2		
	2001	2011	2021
Bani-Mazar	0	0.20	0.20
Dirmouas	0	0.06	0.39
El-Adwa	0	0.04	0.09
El-Fikrih	0.33	0.21	0.35
El-Minya	0.77	1.12	1.44
Magagh	0.05	0.12	0.12
Mallawi	0.20	0.60	2.37
Matai	0	0.04	0.11
New-El-Minya	2.74	0.60	2.60
Samalut	0.15	0.26	0.31

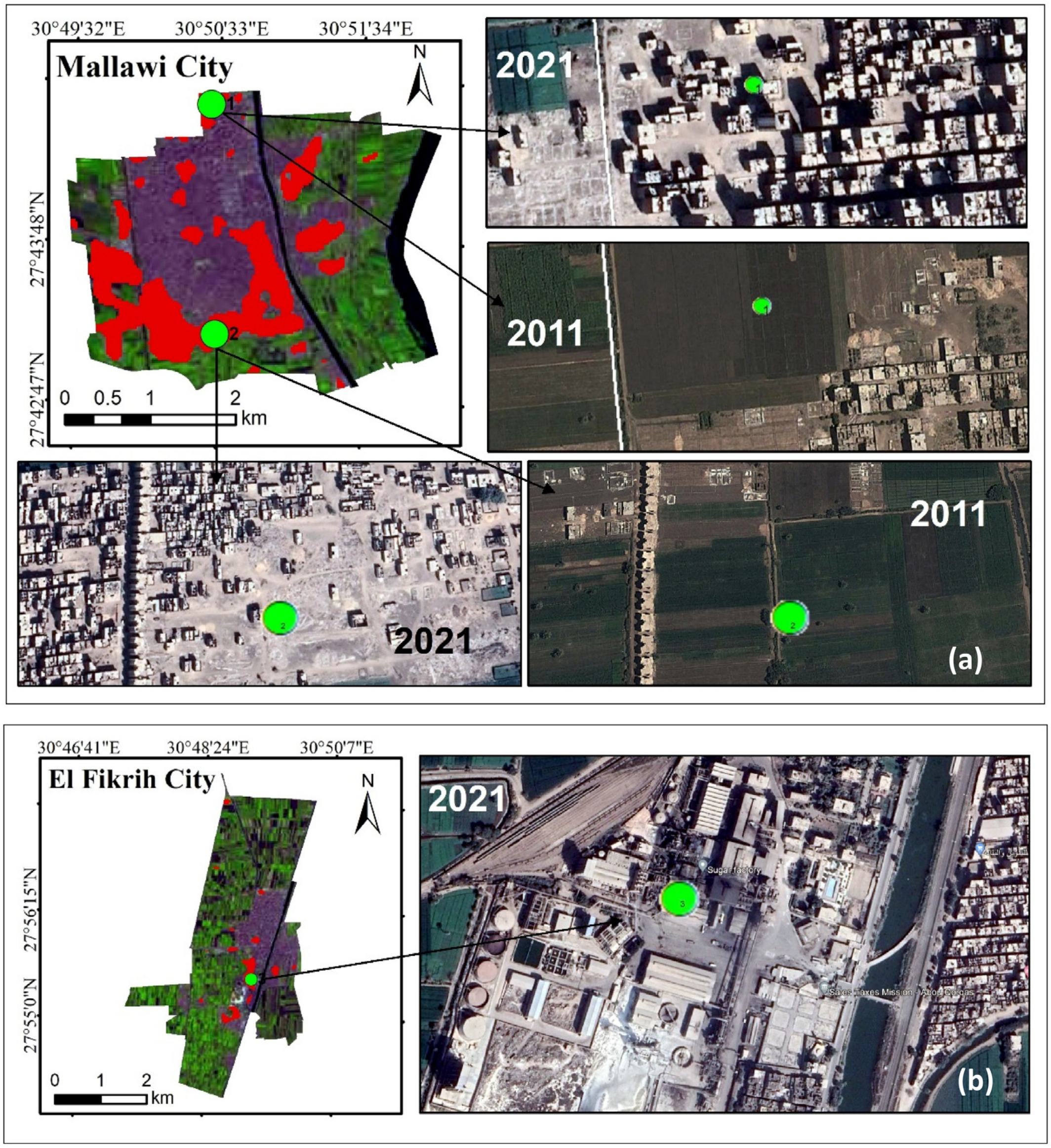

Fig. 4. Example for describing areas of UHIs in a) Mallawi city, b) El-Fikrih city.

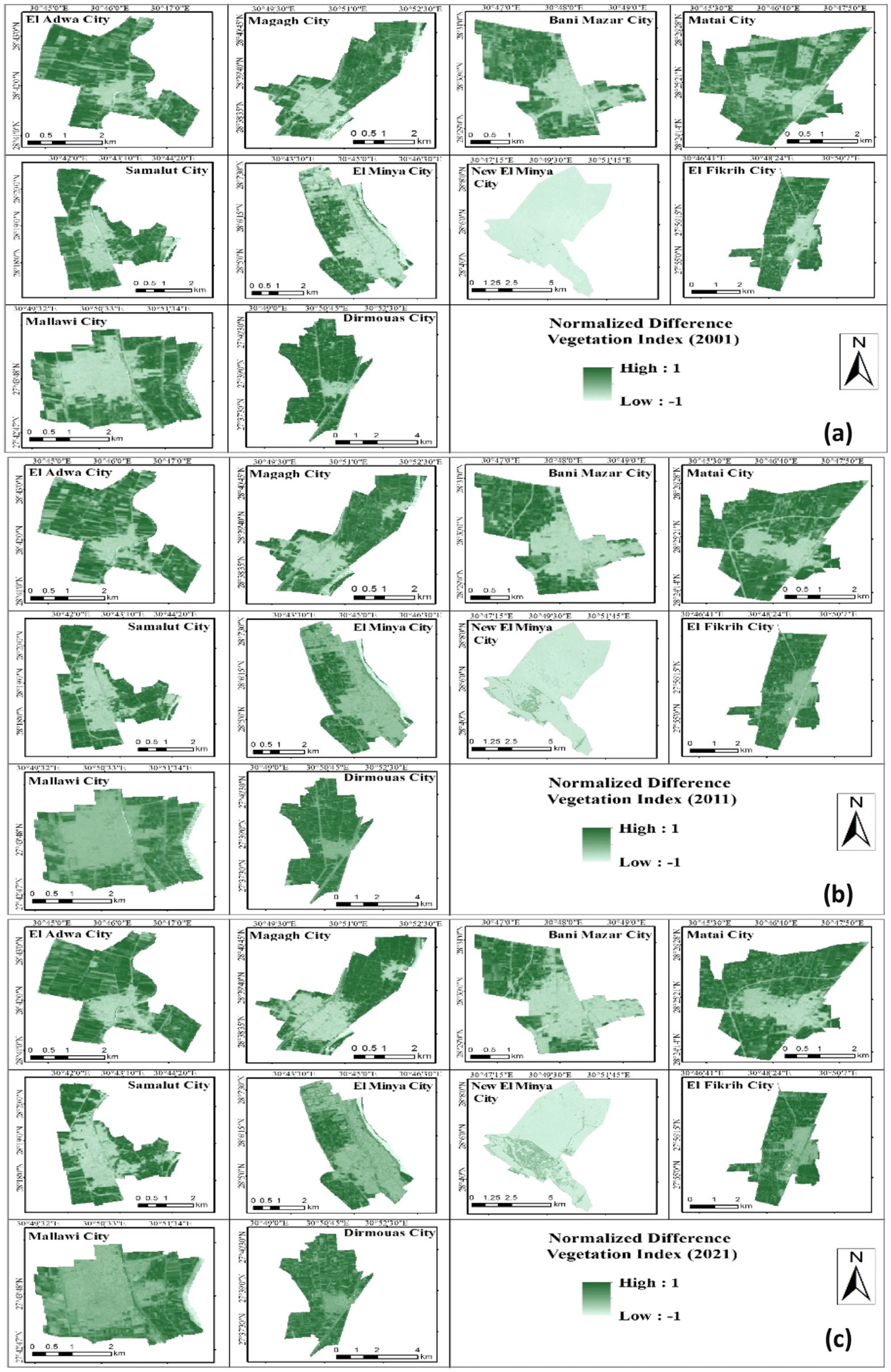

Fig. 5. Variations in NDVI in El-Minya cities in a)2001, b)2011 and c)2021.

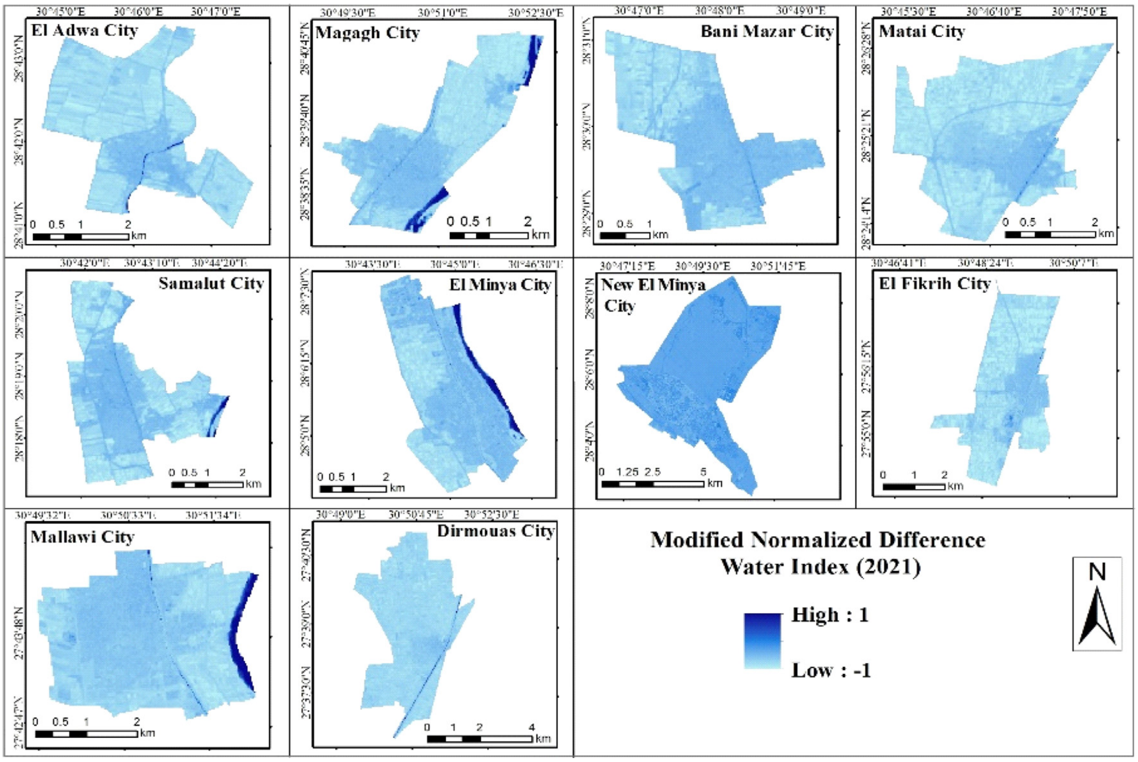

Fig. 6. Variations in NDWI in El-Minya cities in 2021.

Table 4
Statistics of NDVI in El-Minya cities in 2001, 2011, and 2021.

City NDVI	2001				2011				2021			
	MIN	MAX	MEAN	STD	MIN	MAX	MEAN	STD	MIN	MAX	MEAN	STD
El-Minya	−1.0	0.94	0.43	0.25	−0.5	0.96	0.45	0.23	−0.96	0.97	0.68	0.14
El-Fikrih	0.11	0.94	0.64	0.20	0.04	0.92	0.64	0.18	0.40	0.98	0.81	0.12
Mallawi	−1.0	1.00	0.54	0.24	−0.28	0.87	0.48	0.18	−1.0	0.96	0.71	0.11
Dirmouas	0.09	0.94	0.74	0.17	0.04	0.88	0.67	0.14	−1.0	1.00	0.81	0.09
Samalut	−0.57	0.93	0.60	0.23	−1.0	0.94	0.53	0.27	0.25	0.98	0.71	0.18
Bani-Mazar	0.07	0.92	0.55	0.21	0.02	0.95	0.49	0.27	0.41	0.98	0.66	0.17
Magagh	−0.63	0.92	0.59	0.23	−0.77	0.93	0.54	0.26	0.05	1.00	0.72	0.18
El-Adwa	−0.11	0.91	0.65	0.18	−0.08	0.94	0.59	0.22	−0.73	0.98	0.78	0.14
New-El-Minya	0.08	0.73	0.14	0.02	−0.03	0.66	0.08	0.06	0.36	0.90	0.44	0.06
Matai	0.06	0.92	0.61	0.19	0.06	0.96	0.61	0.22	0.44	0.98	0.78	0.15

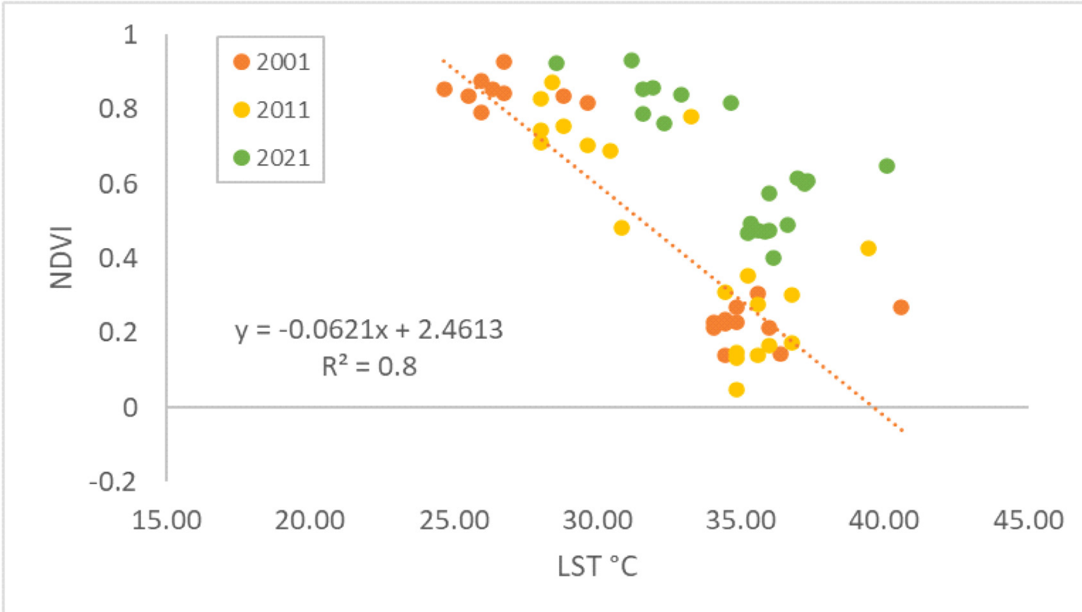

Fig. 7. Scatter diagram with a linear regression between LST and NDVI in 2001, 2011, and 2021.

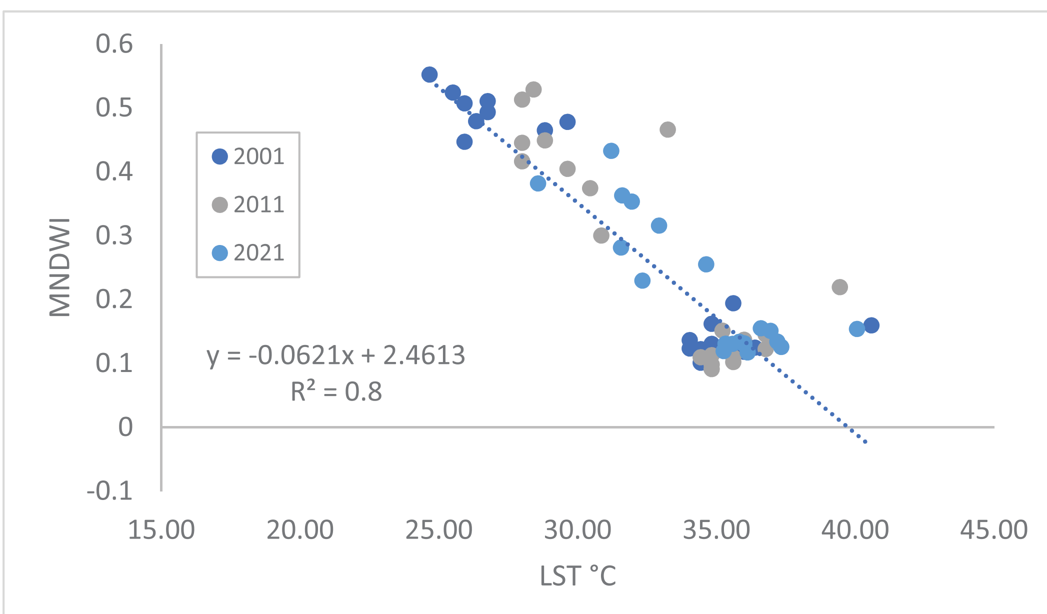

Fig. 8. Scatter diagram with a linear regression between LST and MNDWI in 2001, 2011, and 2021.

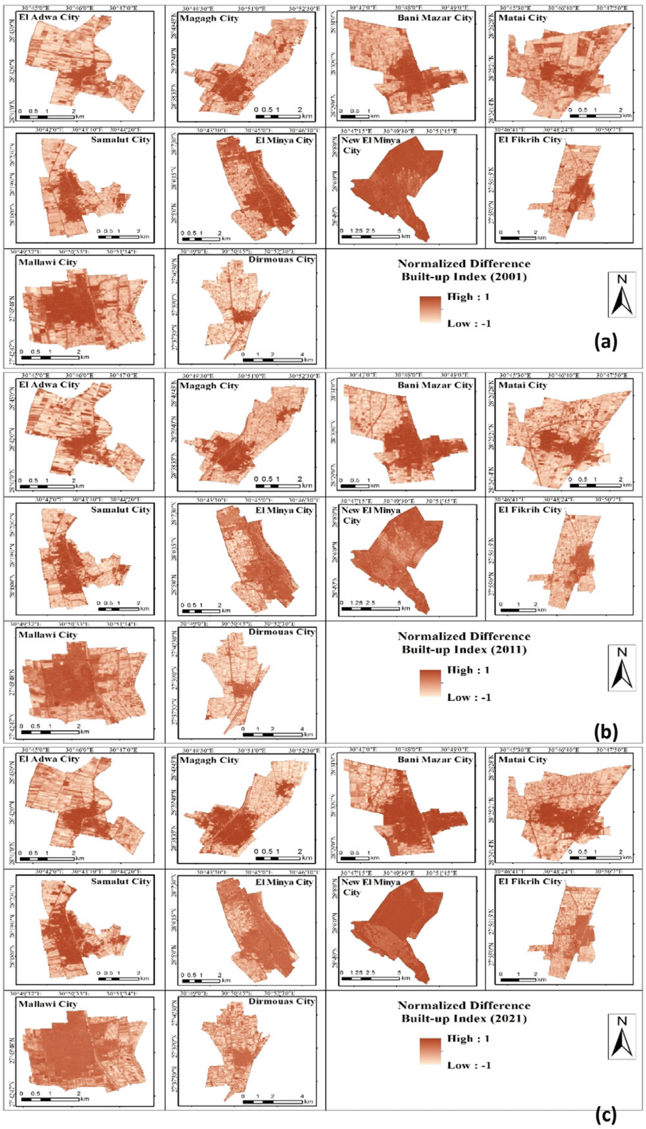

Fig. 9. Changes in NDBI in El-Minya cities in a)2001, b)2011 and c)2021.

acterized by high LST are accompanied by elevated NDBI values. This highlights the effect of urban/built-up land with its impermeable surfaces on increasing LST intensity and raising the potentiality of UHIs formation.

Moreover, land-use in El-Minya cities has a great effect on increasing temperature by direct and indirect ways. Land-use can be represented by several human activities in the cities like transportation and roads network, industry, besides using conditioning systems/heaters. These activities consume huge amounts of energy and consequently generate more anthropogenic heat which strengthens the LST and UHIs. El-Minya governorate has multiple industrial activities such as sugar, and cement, at the eastern side of the government in addition to wood, metal, weaving, and spinning industries. The anthropogenic heat emitted from these activities along with the construction materials of factories, paved streets, and un-shaded open areas can increase the thermal heat stress in the region. Taha et al. (1992) demonstrated that anthropogenic heating in a big city center can form a UHI of up to 2–3 °C during the day and at night. The intensity of anthropogenic heating depends on energy usage patterns, power generation systems as well as transportation.

4. Conclusion

In this research, LST and UHI over the 10-cities of El-Minya Governorate were assessed in July month of 2001, 2011, and 2021 based on thermal and multispectral analyses of Landsat imagery. The spatial distribution and quantitative relationship between LST and the spectral indices (NDVI, MNDWI, and NDBI) were also investigated. High LST accompanied by UHI formation is mainly found in urban/built-up areas as well as bare land/desert. UHIs have a scattered pattern of small boundaries in the cities of El-Minya, New-El-Minya, Mallawi, and Samalout. Results showed that high LST/UHI occurrence probability is lower over cultivated land and moist surfaces. Vegetation cover and surface moisture abundance reduce the surface temperature while the built-up and bare lands have an opposite effect. El-Minya, New-El-Minya, and Mallawi have the highest LST and UHIs than other cities. Among the 10-cities of El-Minya, New-El-Minya city had the highest UHI area nearly 2.74 Km^2 and 2.6 Km^2 in 2001 and 2021, respectively, while in 2011, El-Minya city recorded the greatest UHI area recording 1.12 Km^2. On the contrary, the cities of Bani-Mazar, Dirmouas, El-Adwa, Magagh, and Matai have a very low UHI area and LST as well.

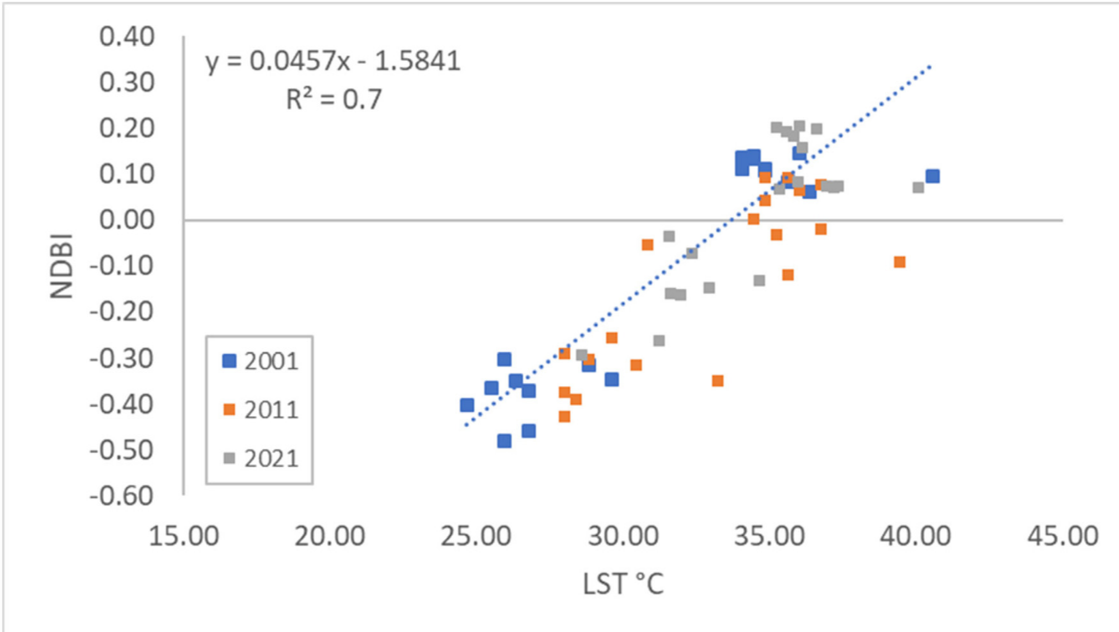

Fig. 10. Scatter diagram with a linear regression analysis between LST and NDBI in 2001, 2011, and 2021.

Finally, urban planning policies should suggest solutions through implementing sustainable adaptation strategies to raise the inhabitants' thermal comfort, increase green and shaded areas. Realizing the UHIs besides assessing the impacts of urban development and thermal stress is the point to start with to solve this problem. The present paper supports urban planners and decision-makers with the necessary information that helps to mitigate the formation of UHIs in El-Minya cities.

Acknowledgement

The authors would like to express their gratitude to the United States Geological Survey (USGS) Earth Explorer for providing the Landsat imagery.

References

Abdelaal, A.M., Sameah, S., Ahmed, A., 2017. Characterization of calcium carbonate rocks, east ElMinya deposits for possibility uses as industrial raw materials. J. Min. Eng. 19 (1).
AbouEl-Magd, I., Ismail, A., Zanaty, N., 2016. Spatial variability of urban heat islands in Cairo City, Egypt using time series of landsat satellite images. Int. J. Adv. Remote Sens. GIS. 5 (3), 1618–1638.
Abdel-Moneim, A., Fernández-Álvarez, J., Abu-El-Ella, E.M., Masoud, A.M., 2016. Groundwater management at west El-Minya Desert Area, Egypt using numerical modeling. J.GEP. 4, 66–76.
Attia, F.A., 1974. Parameters and Characteristics of the Groundwater Reservoir in Upper Egypt. Faculty of Engineering, Cairo University. Ph.D. Thesis.
Chen, X.L., Zhao, H.M., Li, P.X., Yin, Z.Y., 2006. Remote sensing image–based analysis of the relationship between urban heat island and land use/cover changes. J. Remote Sens Environ. 104, 133–146.
Clinton, N., Gong, P., 2013. Modis detected surface urban heat islands and sinks: Global locations and controls. J. Remote Sens. Environ. 134, 294–304.
Deilami, K., Kamruzzaman, M., Liu, Y., 2018. Urban heat island effect: A systematic review of spatio-temporal factors, data, methods, and mitigation measures. Int. J. Appl. Earth Obs. Geoinf. 67, 30–42.
Effat, H.A., Taha, L.G., Mansour, K.F., 2014. Change detection of land cover and urban heat islands using multi-temporal landsat images, application in Tanta City, Egypt. Open J. Remote Sens. Position. 1 (2).
Elbeih, S.F., El-Zeiny, A.M., 2018. Qualitative assessment of groundwater quality based on land use spectral retrieved indices: Case study Sohag Governorate, Egypt. Remote Sens. Appl. Soc. Environ. 10, 82–92. https://doi.org/10.1016/j.rsase.2018.03.001.
El-Bayomi, G., Ali, R.R., 2015. Assessment of urban sprawl on ElMinya archeological sites. Egypt. Res. J. Appl. Sci. 15, 264–270.
ELDeeb, H., El Rawy, M., Habib, E., 2015. Water Resources Management: Case Study of El Minia Governorate. Egypt. J.sci. eng. res. 6 (6).
El-Zeiny, A.M., 2022. Review of land-use impacts on surface water quality in Egypt. J. Indian Soc. Remote Sens. https://doi.org/10.1007/s12524-022-01505-y.
El-Zeiny, A.M., Effat, H.A., 2017. Environmental monitoring of spatiotemporal change in land use/land cover and its impact on land surface temperature in El-Fayoum governorate. Egypt. J. Remote Sens Appl. 8, 266–277.
El-Zeiny, A., Effat, H., Mansou, R.K., Shahin, A., Elwan, K., 2022. Geo-environmental monitoring of coastal and land resources of Port Said Governorate, Egypt. Egypt. J. Remote Sens. Space Sciences 25 (1), 157–172. https://doi.org/10.1016/j.ejrs.2022.01.009.
Grimm, N.B., Faeth, S.H., Golubiewski, N.E., Redman, C.L., Wu, J., Bai, X., Briggs, J.M., 2008. Global change and the ecology of cities. Science. 319, 756–760.
Huang, Q., Lu, Y., 2018. Urban heat island research from 1991 to 2015: A bibliometric analysis. Theor. Appl. Climatol. 131, 1055–1067.
Kovats, R.S., Hajat, S., 2008. Heat stress and public health: A critical review. Annu. Rev. Public Health. 29, 41–55.
Kumar, K.S., Bhaskar, P.U., Padmakumari, K., 2012. Estimation of land surface temperature to study urban heat island effect using Landsat ETM+ image. Int. J. Eng. Sci. Technol. 4 (02), 771–778.
Li, J., Song, C., Cao, L., Zhu, F., Meng, X., Wu, J., 2011. Impacts of landscape structure on surface urban heat islands: A case study of Shanghai. China. Remote Sens Environ. 115, 3249–3263.
Li, X., Zhou, Y., Asrar, G.R., Imhoff, M., Li, X., 2017. The surface urban heat island response to urban expansion: A panel analysis for the conterminous United States. Sci. Total Environ. 605, 426–435.
Li, Y., Zhang, H., Kainz, W., 2012. Monitoring patterns of urban heat islands of the fast–growing Shanghai metropolis, China: using time–series of Landsat TM/ETM+ data. Int. J. Appl Earth Obs Geoinf 19, 127–138.
Liu, L., Zhang, Y., 2011. Urban heat island analysis using the Landsat TM data and ASTER data: A case study in Hong Kong. Remote Sens. 3, 1535–1552.
Lu,Y., Feng, P., Shen, C. Sun, J. 2009. Urban heat island in summer of Nanjing based on TM data. In proceedings of 2009 Joint Urban Remote Sensing Event, Shanghai, China, 20–22 May 2009, 1–5.
Miky, Y.H., 2019. Remote sensing analysis for surface urban heat island detection over Jeddah. Saudi Arabia. Appl Geomat. 11, 243–258.
Oke, T.R., 1982. The energetic basis of the urban heat island. Q. J. R. Meteorol. Soc. 108, 1–24.
Patz, J.A., Campbell-Lendrum, D., Holloway, T., Foley, J.A., 2005. Impact of regional climate change on human health. Nature 438, 310–317.
Peng, S., Piao, S., Ciais, P., Friedlingstein, P., Ottle, C., Breon, F.-M., Nan, H., Zhou, L., Myneni, R.B., 2012. Surface urban heat island across 419 global big cities. Environ. Sci. Technol. 46, 696–703.
Renard, F., Alonso, L., Fitts, Y., Hadjiosif, A., Comby, J., 2019. Evaluation of the Effect of Urban Redevelopment on Surface Urban Heat Islands. Remote Sens. 11, 299.
Rizwan, A.M., Dennis, L.Y.C., Liu, C., 2008. A review on the generation, determination and mitigation of urban heat island. J. Environ. Sci. 20, 120–128.

Roupioz, L., Nerry, F., Colin, J., 2018. Correction for the impact of the surface characteristics on the estimation of the effective emissivity at fine resolution in urban areas. Remote Sens. 2018 (10), 746.

Santamouris, M., Cartalis, C., Synnefa, A., Kolokotsa, D., 2015. On the impact of urban heat island and global warming on the power demand and electricity consumption of buildings—A review. Energy Build. 98, 119–124.

Seto, K.C., Güneralp, B., Hutyra, L.R., 2012. Global forecasts of urban expansion to 2030 and direct impacts on biodiversity and carbon pools. Proc. Natl. Acad. Sci. USA 109, 16083–16088.

Shepherd, J.M., 2005. A review of current investigations of urban-induced rainfall and recommendations for the future. Earth Interact. 9, 1–27.

Sigman, R., Hilderink, H., Delrue, N., Braathen, N.A., Leflaive, X., 2012. OECD Environmental Outlook to 2050. OECD Environ. Outlook.

Sobrino, J.A., Caselles, V., Becker, F., 1990. Significance of the remotely sensed thermal infrared measurements obtained over a citrus orchard. ISPRS Photogramm. Eng. Remote Sens. 44, 343–354.

Sobrino, J.A., Raissouni, N., 2000. Toward remote sensing methods for land cover dynamic monitoring, application to Morocco. Int. J. Remote Sens. 21, 353–366.

Sobrino, J.A., Jiménez-Muñoz, J.C., Paolini, L., 2004. Land surface temperature retrieval from LANDSAT TM5. Remote Sens. Environ. 90 (4), 434–440.

Stathopoulou, M., Cartalis, C., 2007. Daytime urban heat islands from Landsat ETM+ and Corine land cover data: an application to major cities in Greece. Solar Energy. 81, 358–368.

Taha, H., Akbari, H., Sailor, D., Ritschard, R. 1992. Causes and effects of heat islands: sensitivity to surface parameters and anthropogenic heating. Lawrence Berkeley Laboratory Report No. 29864.

UN. United Nations Department of Economic Social Affairs Population Division. World Urbanization Prospects: The 2018 Revision; Online Edition; United Nations: New York, NY, USA, 2018.

Voogt, J.A., Oke, T.R., 2003. Thermal remote sensing of urban climates. Remote Sens. Environ. 86, 370–384.

Xu, H., 2006. Modification of normalised difference water index (NDWI) to enhance open water features in remotely sensed imagery. Int. J. Remote Sens. 27 (14), 3025–3033. https://doi.org/10.1080/01431160600589179.

Zhang, J., Wang, Y., Wang, Z., 2007. Change analysis of land surface temperature based on robust statistics in the estuarine area of Pearl River (China) from 1990 to 2000 by Landsat TM/ETM+ data. Int. J. Remote Sens. 28 (10), 2383–2390.

Zhao, S., Liu, S., Zhou, D., 2016. Prevalent vegetation growth enhancement in urban environment. Proc. Natl. Acad. Sci. USA 113, 6313–6318.

Zhou, D., Xiao, J., Bonafoni, S., Berger, C., Deilami, K., Zhou, Y., Frolking, S., Yao, R., Qiao, Z., Sobrino, J.A., 2019. Satellite remote sensing of surface urban heat islands: progress, challenges, and perspectives. Remote Sens. 11, 48.

Liu, X., Ming, Y., Liu, Y., Yue, W., Han, G., 2022. Influences of landform and urban form factors on urban heat island: Comparative case study between Chengdu and Chongqing. Sci. Total Environ. 820, 153395.

Faisal, A., Al-Kafy, A., Al-Rakib, A., Akter, K.S., Jahir, D.M.A., Sikdar, M.S., Ashrafi, T.J., Mallik, S., Rahman, M.M., 2021. Assessing and predicting land use/land cover, land surface temperature and urban thermal field variance index using Landsat imagery for Dhaka Metropolitan area. Environ. Challenges 4, 100192.

Ramaiah, M., Ram Avtar, R., Rahman. M.M. 2020. Land Cover Influences on LST in Two Proposed Smart Cities of India: Comparative Analysis Using Spectral Indices. Land, 9, 292; 10.3390/land9090292.

Artis, D.A., Carnahan, W.H., 1982. Survey of emissivity variability in thermography of urban areas. Remote Sens. Environ. 12 (4), 313–329.

Shahfahad, M.W., Naikoo, A.R., Towfiqul Islam, M.d., Mallick, J., Rahman, A., 2022. Land use/land cover change and its impact on surface urban heat island and urban thermal comfort in a metropolitan city. Urban Climate 41, 101052.